Risk of failure during gait for direct skeletal attachment of a femoral prosthesis: A finite element study

Benedikt Helgason [b], Halldór Pálsson [a], Tómas Philip Rúnarsson [a], Laurent Frossard [c], Marco Viceconti [d]

[a] *Department of Mechanical and Industrial Engineering, Faculty of Engineering, University of Iceland, Iceland*
[b] *School of Science and Engineering, Department of Biomedical Engineering, Reykjavík University, Iceland*
[c] *Institute of Health and Biomedical Innovation, School of Engineering Systems, Queensland University of Technology, Australia*
[d] *Laboratorio di Tecnologia Medica, Istituti Ortopedici Rizzoli, Bologna, Italy*

(Manuscript as published: Helgason B, Pálsson H, Taddei F, Rúnarsson T, Frossard F, Viceconti M, Brynjólfsson S. Risk of failure during gait for direct skeletal attachment of a femoral prosthesis: A finite element study. 2009. Medical Engineering and Physics. 31. p 595–600)

ABSTRACT

Direct skeletal attachments for transfemoral amputees have been the subject of clinical trials since the early nineties. This method of attachment allows the amputee an unrestricted range of motion around the hip joint, better sitting comfort, improved sensory feedback through osseoperception, improved limb control and reduced soft tissue problems. However, the length of the rehabilitation period is perceived as a shortcoming by the amputees and the clinicians. The aim of the present study is to estimate the risk of failure during gait, for a patient with direct skeletal attachment of a femoral prosthesis, using finite element analysis (FEA).

Material properties and loads were derived from subject-specific data and implant stability assumed secured by bone ingrowth into a porous implant surface. A simplified FEA was used to optimize the implant geometry with respect to load bearing capacity. The resulting geometry was then implemented in a subject-specific FE study. The results indicate that the risk of failure for the implant system is approximately three times greater than what can be expected for an intact femur.

The main conclusion, based on the risk of failure factors calculated, is that it is likely that a porous-coated implant could be beneficial for osseointegrated fixation. It is also suggested that the proposed methodology can be used in future studies exploring the mechanical stability of osseointegrated fixation in the view of improving direct skeletal attachments for lower limb amputees.

KEYWORD

Finite element analysis, Femur, Direct skeletal attachment, Optimization, Orthopedic implants

INTRODUCTION

Direct skeletal attachments for transfemoral amputees have been the subject of clinical trials since the early nineties [3,11,4,1]. The most common surgical procedure involves a fixation that is implemented in two stages [4,42]. First, an implant is fitted into the distal end of the residual limb. Then, an undisturbed osseointegration is enabled for a minimum of 6 months. Second, a transcutaneous abutment is attached to the implant. A few weeks after the rehabilitation program starts. It includes gradually increased load bearing exercises and prosthetic activity until the bonding between the implant and bone is sufficiently strong to support the amputees full body weight in walking [13,42,30]. Currently, this program lasts approximately 12 months. This method of prosthetic attachment allows the amputee unrestricted range of motion around the hip joint, better sitting comfort, improved sensory feedback through osseoperception, improved limb control and reduced soft tissue problems. Consequently amputees can walk further and be more active than amputees fitted with a conventional prosthesis [35,14,15]. All combined, these outcomes contribute significantly to improve the quality of life of these amputees. However, the length of the rehabilitation period is perceived as a shortcoming by the amputees and the clinicians. This could prevent a more general adoption of this promising technique into clinical practice.

Threaded implants, which are currently the method of fixation for direct skeletal attachments, are designed to securely transfer axial loads but have limited stability against torsion as pointed out by [3]. The presence of considerable torsional loads during gait has been verified experimentally by e.g. [9,25,10,46]. Additionally the risk of stress concentration around the implant threads leading to bone resorption is well known. Consequently, porous-coated implants might be an avenue to explore in further developments of the osseointegrated fixations.

Shortening the rehabilitation program requires a better understanding of the implant mechanical stability. One

way to achieve this is by using finite element analysis (FEA) which is increasingly gaining recognition from clinicians as tool to for example predict the outcome of an orthopedic surgery [39,37]. Several studies have provided experimental validation of FE models predicting mechanical response of intact bone on the organ scale [20,7,27,26,38,29,6,12,36,16]. However, the development of bone ingrowth into a porous implant surface depends on biological as well as mechanical factors. This makes experimental validation of FE models of the bone implant interface particularly challenging. So far, mainly numerical studies predicting long term implant stability have been published [40,41]. The extent of bone ingrowth around an implant system, and thus shear strength of the bone implant interface, has to be taken, consequently, as a study variable in numerical simulations for osseointegrated fixations.

The stress and strain patterns around threaded implants for femoral attachments have been studied by several investigators [22,24,25,43–45]. In these studies the authors have used material properties and loads from the literature or not conducted subject-specific analysis. The main purpose of the present study, however, is to estimate the risk of failure during gait for an amputee fitted with an osseointegrated fixation, where material properties and loads are derived from subject-specific data and implant stability secured by a porous implant surface instead of a thread. The specific objectives are twofold. Firstly, to optimize the geometry of the implant system with respect to load bearing capacity using a simplified FE model. Secondly, to estimate the risk of failure during gait for this implant system using a subject-specific FE model.

MATERIALS AND METHODS

Problem description

CT-scans taken postoperatively are generally not available for patients fitted with direct skeletal femoral attachments. Hence, to allow for a realistic numerical simulation in the subject-specific study, CT-data for an intact femur was taken from Helgason et al. [16] (subject 1: male 51 years old, 1.75 m and 75 kg). In the present study the CT data was used to construct a FE model of an amputated femur from a given clinical case (subject 2: male 45 years old, 1.72 m and 80 kg) for which gait analysis data was available. The length of the residual limb for this patient measured 280 mm from the greater trochanter to the distal end of the bone. The same applied for the subject-specific FE model.

Simplified FE model

For the optimization part of this study the geometry of the femur was modeled as a hollow cylindrical shaft with a round end plate attached to it. This was done to limit computational cost but also because the meshing procedures for the subject-specific model could not be fully automated. The implant was assumed to have a hollow conical shape. To allow for a realistic simulation of geometry and material properties, average inner and outer diameter of the femoral shaft were estimated from the CT data using a threshold of HU = 200 for determining the boundary between bone and soft tissue. The resulting values for outer and inner radii were R =16mm and r = 8 mm, respectively. The radius of the endplate was set to e = 60 mm which was the estimated eccentricity of vertical load calculated from the gait analysis data as described later. A schematic illustration of this structural problem along with the relevant model parameters is illustrated in Fig. 1(a).

To simplify mesh procedures the abutment was modeled as a hollow cylinder with an inner radius of r4 = 1 mm. The skeletal part of the simplified FE model consisted of 6256 “20-node” hexahedral elements but the implant and abutment were modeled with 2880–6240 “20-node” hexahedral solid elements depending on the values of L3 and L5. The bone implant interface was modeled with 208–688 pairs of “8-node” contact and target surface elements but the number of contact pairs depends on the length of the implant (L3). The contact behavior was switched to bonded for all contact pairs to simplify the optimization process. The distal end of the abutment, which corresponds to the location of the load cell in the gait analysis experiment, was fixed at all nodes.

Subject-specific FE model

The subject-specific FE model was built from the CT data for subject 1 in a three-step process:

1. CT data segmentation and three-dimensional bone surface extraction which was imported into a commercial FE software (Ansys, Inc., USA, V10.0) where the implant and abutment were modeled. Geometry of the implant system was based on the results from the optimization of the simplified model.
2. Construction of a FE mesh (Ansys Workbench) using “10-node” tetrahedral solid elements.
3. Mapping of inhomogeneous material properties onto the FE mesh using the NI method [16].

Average element edge length for the bone, implant and abutment was set to 2.7 mm. This resulted in the bone being meshed with 71,399 elements and 105,281 nodes and the metal parts with 10,050 elements and 16,162 nodes. For the purpose of comparison, a FE mesh of the intact femur was also constructed (average element edge length 3.3 mm, 85445 elements and 125956 nodes. The bone implant interface was modeled with 1218 and 1262 “6-node” contact and target elements, respectively. Partial bone ingrowth into the pores of the implant surface was simulated with bonded contact for a given percentage (Acon) of the contact pairs but assuming that frictionless sliding applied for the rest of them.

Material properties

The implants were assumed to be made from Ti–6Al–4V alloy with a porous-coated surface. Young's modulus and Poisson's ratio for this material were set to 110 GPa and 0.3, respectively. The same material properties were assigned to the abutment. Failure was assumed to be present if Von Mises equivalent element stress reached the fatigue limit of ASTM grade 5Ti–6Al–4V alloy. This value was set to _f,Ti = 493 MPa.

In the present study the following modulus density relationship was used to relate Young's modulus to apparent density:

$$E(\text{GPa}) = 6.85(\rho_{app}(\text{g/cm}^3))^{1.49} \quad (1)$$

A calibration between CT numbers and ash density was available for the dataset [36], but the following relationship from [17] was used to transform ash density to apparent density.

$$\rho_{app} = \frac{\rho_{ash}}{0.55} \quad (2)$$

For the subject-specific FE model, Young's modulus was applied to the model using the NI material assigning method introduced by [16], thus assigning different Young's modulus to each node in the model. Using the NI method the highest correlation between strain measurements and simulation for the present bone specimens was achieved for the methods tested by [16,36]. Apart from mapping the Young's modulus information more accurately to each finite element in the mesh than conventional mapping strategies, countermeasure against partial volume artifacts in the CT data are included in the NI method. For the simplified FE model the Young's modulus for bone was set to a constant value of E =21,348MPa, which was the average value of E in the femoral shaft around the implant determined from the subject-specific FE model. Bone in both cases was assumed to be isotropic with a Poisson's ratio of _ = 0.3. Yield strain has not been correlated thoroughly to apparent density in the literature. However, according to [19] indications exist to suggest that yield strain is relatively independent of apparent density and is often reported in the range of 0.6–1.2%. A value of εy,b = 0.9% was assumed to represent a catastrophic failure of bone in the present study.

Average bone implant interface strength for porous Titanium implants, retrieved 3 months postoperatively or later, was reported in the range of 3.5–22.1 MPa by [5,21,8,34]. In the optimization of the simplified model it was assumed that bone implant interface failure was present if element stresses in the contact elements reached 8 MPa. Fracture strength for the bone implant interface in the subject-specific FE model was not specifically defined. Failure at the interface, in this case, was assumed to be present if equivalent Von Mises strains exceeded 0.9%.

Load

Loads during gait were measured directly for subject 2 by placing a load cell at the distal end of the residual limb according to the protocol described in [9,10,23]. Measured load cell forces and moments from a single gait cycle are illustrated in Fig. 2. For the simplified FE model a point load P was assigned to the model. The eccentricity of this load, with respect to the center of the abutment, was calculated as

$$e = \frac{MAX\left(\sqrt{M_{x,t}^2 + M_{y,t}^2}\right)}{F_{z,t}} \quad (3)$$

where Mx,t and My,t are the measured bending moments at time t in the gait cycle, about the medial–lateral and anterior–posterior axes, respectively (Fig. 2). Fz,t is the corresponding measured normal force at time t.

Loads were applied to the subject-specific FE model at three anatomical sites: femoral head, trochanter major and trochanter minor as illustrated in Fig. 3(b). At all the sites a set of three orthogonal forces was applied but their magnitude was determined by using a simplified 3D FE beam model of the bone, where the femur was modeled as a column with consoles corresponding to the eccentricity of the three anatomic sites with respect to the femoral shaft (Fig. 3(a)). The 3D beam model was then supported against translation in three orthogonal directions at the three anatomic sites and measured gait loads applied to the distal end of beam model. Reactions at the supports of the beam model where then found with FE simulation of one gait cycle and then afterwards applied in the FE analysis of the subject-specific model, which was supported at the distal end of the abutment. All measured forces and moments in the gait analysis data were multiplied by a factor of 75/80 before they were applied in the FE analysis to account for the weight difference between subjects 1 and 2.

FE-analysis

The FE simulations (large sliding contact analysis) were implemented using commercial software (Ansys, Inc., USA, V10.0). Control parameters for the contact algorithm where left as defaults for both the simplified model and the subject-specific model, as determined by the FE software except that the contact force tolerance factor was set to 5.0, which was a value found to positively influence numerical stability in the large sliding contact study of Bernakiewicz and Viceconti [2]. The default solver of the software was used.

The optimization for the simplified FE model was setup as the maximization of load bearing capacity P as a function of the geometrical variables, r1, r2, r3 and L5, i.e.

$$MAX\left(P(r_1, r_2, r_3, L_5)\right) \quad (4)$$

while satisfying the constraints

$$r_2 - r_1 \geq 0 \ mm$$
$$r_3 - r_1 \geq 1.5 \ mm$$
$$R - r_2 \geq 1.5 \ mm$$
$$r_1 - r \geq 0 \ mm$$
$$r_2 - r_3 \geq 0 \ mm$$
$$L_5 \geq 5.0 \ mm$$
$$L_3 - L_5 \geq 5.0 \ mm$$
$$\in_{vm,b} \leq \in_{y,b} = 0.9\%$$
$$\sigma_{vm,Ti} \leq \sigma_{f,Ti} = 493 \ MPa$$
$$\tau_{\text{int}erface} \leq \tau_{\max} = 8 \ MPa$$

The geometrical constrains were defined to secure a minimum material thickness for bone, implant and abutment, but also to secure a realistic taper for the medullary canal after reaming. $\in_{vm,b}$ is the average Von Mises equivalent element strain in bone, $\sigma_{vm,Ti}$ is the Von Mises equivalent element stress in the titanium alloy, and $t_{interface}$ is the bone implant interface shear stress as calculated in the FE simulations.

A stochastic optimization method known as the (1 + 1) Evolution Strategy [32] was used for optimization. The algorithm, which was implemented in MATLAB Version 7.1, is in principle a randomized hill climber, using a Gaussian search distribution with an adaptive standard deviation. Optimum search was carried out in two trials with 100 FE simulations, in each trial, to get two independent search paths in the optimum search. After each FE simulation the objective function in Eq. (4) was evaluated and the search strategy adapted if necessary. To investigate the influence of implant length on the outcome of the optimization, optimum search was carried out for L3 = 40–120 mm.

The FE analysis for the subject-specific model was carried out for a complete gait cycle in 0.06 s steps for three different values of the bone implant contact percentage, i.e. Acon = 20, 70 and 100%. For Acon = 20 and 70% the FE analysis was carried out 20 times, randomly distributing the bone implant contact prior to each simulation with a built in MATLAB function. Risk of failure was defined as

$$RF_b = \frac{MAX(\in_{vm,b})}{0.9\%} \quad (5)$$

and

$$RF_{Ti} = \frac{MAX(\sigma_{vm,Ti})}{493 \ MPa} \quad (6)$$

for bone and implant/abutment respectively. The risk of failure for bone was calculated for a region of interest (ROI) that was defined to extend from a plane approximately 10 mm below the trochanter minor to the distal end of the residual limb. Average risk of failure with standard deviation was then calculated for each value of the bone implant contact percentage Acon. For the purpose of comparison one simulation was carried out for an intact femur, i.e. without the implant system. Risk of failure was calculated for the same region of interest in this case.

RESULTS

Simplified model

Results from the optimization are presented in table 1. Maximum load bearing capacity was achieved for an implant length of L3=80 mm. A parameter study showed however, that the objective function in eq. (4) was relatively insensitive to changes in the geometrical variables in the vicinity of the optimum solution. In all cases the bone implant interface strength ($t_{interface}$) was the limiting factor for the load bearing capacity.

Subject-specific model

Based on the results from the optimization the geometrical variables for the implant system of the subject-specific model were set to r1 =8mm, r2 =10mm, r3 = 6.5 mm, r4 =0mm and L5 =55mm. Calculated average risk of failure from 20 simulations for the amputated femur and the intact femur are presented in Fig. 4. The calculated maximum average risk of failure derived from this analysis is presented in Table 2.

The highest risk of failure in bone was always present at the bone implant interface for the amputated femur. For Acon = 100% the risk of failure was determined by a failure in a single element at the posterior side of the bone implant interface. For A = 20 and Acon =70% the location of the failure zone depended on the bone contact pattern. The maximum risk of failure in the implant/abutment was always present in the abutment. To allow for a comparison with the literature, Von Mises stresses in bone in the ROI and Acon =100% is illustrated in Fig. 5. Maximum Von Mises stress (61.474 MPa) was found on the outer surface at the proximal end and at the anterior side of the ROI in this case. The maximum risk of failure for the intact femur (RFb = 34%) was found to be on the outer surface of the bone in the proximal part of the ROI.

DISCUSSION

The aim of the present study was to estimate the risk of failure during gait for a patient with a direct skeletal attachment of a femoral prosthesis. The maximum risk of failure for the bone and porous implant system was on average found to lie in the range of 97–112% depending on the bone implant contact percentage compared to 34% for an intact femur (Table 2). Failure according to the results is thus approximately three times more likely to occur in the amputated femur than in the intact femur.

Direct comparison of the results from the present study to the literature is difficult because of inter-study methodological differences and the subject-specific

nature of the results. However, in the studies of [44,45] three-dimensional subject-specific FE models were used to calculate the stress patterns due to loads derived from daily activities, around different types of threaded implants. Zhang et al. [45] reported Von Mises stresses below 30 MPa in bone for all of the implants they studied. However, they did not report on the strain levels. Xu et al. [44] reported Von Mises stresses in bone below 50 MPa for all the implants geometries that they studied. They used four-node tetrahedral elements to allow for dense meshing around the implant threads and reported stresses at a given distance from the implant threads to avoid stress peaks, but the authors did not report why they found this reasonable. Maximum strain in bone of 0.15% was reported which is lower than the maximum strains found in the present study (0.87% in ROI for Acon = 100%). In the present study we found the highest stresses in bone around the implant to be 47.2 MPa on the outer posterior surface of the bone at the proximal end of the implant. Higher Von Mises stresses in bone (61.474 MPa) were found in the proximal part of the diaphysis (Fig. 5). Stress levels in the present studies are therefore comparable to similar studies but the strain levels are not based on comparison with a single value reported in the literature.

The accuracy of the FE model for the femoral specimen used in the subject-specific part of the present study, along with the material mapping strategy, was studied by [36,16]. The root mean square error in surface strain prediction for this model is below 10% when using the elasticity density relationship introduced by [28] and the NI material mapping procedure. Additionally loads were derived from direct measurements which should lead to realistic boundary conditions for the FE model for daily activities. However uncertainties with respect to using gait loads from one individual do analyze another exist but there was no way to avoid that in the present study.

Uncertainties in the FE analysis are also present for the load transfer at the bone implant interface. The results indicate, however, that as soon as the implant system is introduced the predicted risk of failure increases drastically. The average risk of failure (Fig. 4) is relatively independent upon bone implant contact (Acon) which is contradictory to what could be expected. However, the standard deviation of the maximum risk of failure (Table 2) increases with decreasing bone implant contact, which means that bone ingrowth is vital for increasing the probability of successful implantation.

We defined failure in bone by a simple strain based failure criteria which has not been experimentally validated. The risk of failure might thus be over or under estimated in the present study. Quantifying this uncertainty is difficult since damage repair ability of bone is a time dependent biological process, driven by a signal that is currently not fully understood. The taper and thickness of the implant were kept as variables in the optimization process to allow for some smoothing of the stress patterns at the bone implant interface but a simple parameter study indicated that that this was only the case for the taper, i.e. the difference between r1 and r2 but a change in the wall thickness of the implant had limited effect. This is most likely because the implant with the abutment inserted has much higher flexural rigidity than the surrounding bone. This could be changed however by e.g. radial cuts into the walls of the implant which is a well known method for stress/strain relief. Apart from these uncertainties torsional load was not included in the optimization of the simplified FE model. This was done to simplify the optimization process. As a result further shape optimization of the bone implant system might be possible.

CONCLUSIONS

This study relies on the assumption that the clinical case considered presented good bone quality and firm osseointegration. Given these assumptions, the main conclusion based on the risk of failure factors is, that it is likely that a porous-coated implant could be beneficial for osseointegrated fixation, with the similar limitations in use as patients fitted with threaded implants are currently subjected to [35]. This is our conclusion bearing in mind that the implant system design in the present study could be improved by stress relieving measures and further shape optimization. A formal demonstration of the benefits of porous-coated implants will require studies using similar FE models to compare both types of fixations for a large number of subjects.

ACKNOWLEDGEMENTS

This work is supported financially by the Icelandic Research Council. The authors wish to express their gratitude to Fulvia Tad dei (Istituti Ortopedici Rizzoli, Bologna, Italy), Kerstin Hagberg, Eva Haggstrom and Dr Rickard Branemark (Centre of Orthopaedic Osseointegration, Sahlgrenska University Hospital, Goteborg, Sweden) for their contribution to this study.

CONFLICT OF INTEREST STATEMENT

The authors confirm that their professional judgement is not influenced by factors, such as financial gain, that could bias their work.

REFERENCES

[1] Aschoff H, Grundei H. The endo-exo-femurprosthesis: a new concept of prosthetic rehabilitation engineering following thigh-amputation—some cases and early results. In: International society for prosthetics and orthotics 11th world congress, 2004. 2004. p. 103.

[2] Bernakiewicz M, Viceconti M. The role of parameter identification in finite element contact analyses with reference to orthopaedic biomechanics applications. Journal of Biomechanics 2002;35(1):61–7.

[3] Brånemark R, Öhrnell L-O, Nilsson P, Thomsen P. Biomechanical characterization of osseointegration during healing: an experimental in vivo study in the rat. Biomaterials 1997;18:969–78.
[4] Brånemark R, Brånemark P-I, Rydevik B, Myers R. Osseointegration in skeletal reconstruction and rehabilitation: a review. Journal of Rehabilitation Research and Development 2001;38(2):175–81.
[5] Clemow AJT, Weinstein AM, Klawitter JJ, Koenman J, Anderson J. Interface mechanics of porous titanium implants. Journal of Biomedical Materials Research 1981;15(1):73–82.
[6] Couteau B, Mansat P, Estivalézes E, Darmana R, Mansat M, Egan J. Finite element analysis of the mechanical behavior of a scapula implanted with glenoid prosthesis. Clinical Biomechanics 2001;16(7):566–75.
[7] Dalstra M, Huiskes R, van Erning L. Development and validation of a three-dimensional finite element model of the pelvic bone. Journal of Biomechanical Engineering 1995;117(3):271–8.
[8] Dhert WJ, Klein CP, Wolke JG, van der Velde EA, de Groot K, Rozing PM. A mechanical investigation of fluorapatite, magnesiumwhitlockite, and hydroxylapatite plasma-sprayed coatings in goats. Journal of Biomedical Materials Research 1991;25(10):1183–200.
[9] Frossard L, Beck J, Dillon M, Evans J. Development and preliminary testing of a device for the direct measurement of forces and moments in the prosthetic limb of transfemoral amputees during active of daily living. Journal of Prosthetics and Orthotics 2003;15(4):135–42.
[10] Frossard L, Stevenson N, Smeathers J, Häggström E, Hagberg K, Sullivan J, et al. Monitoring of the load regime applied on the osseointegrated fixation of a trans-femoral amputee: A tool for evidence-based practice. Prosthetics and Orthotics International 2007;32(1):68–78.
[11] Gunterberg B. Osseointegration prosthesis in lower limb amputation—the development of a new concept. In: Proceedings of the IXth world congress of society of international prosthetics and orthotics. 1998. p. 137–9.
[12] Gupta S, van der Helm FCT, Sterk JC, van Keulen F, Kaptein BL. Development and experimental validation of three dimensional finite element model of the human scapula. Proceedings of the institution of mechanical engineers, part H, vol. 218. Journal of Engineering in Medicine 2004:127–42.
[13] Hagberg K. Chapter 25: physiotherapy for patients having a trans-femoral amputation. In: Brånemark P-I, editor. The osseointegration book—from calvarium to calcaneus. Quintessenz Verlag-GmbH; 2005. p. 477–87.
[14] Hagberg K, Haggstrom E, Uden M, Brånemark R. Socket versus bone-anchored trans-femoral prostheses: hip range of motion and sitting comfort. Prosthetics and Orthotics International 2005;29(2):153–63.
[15] Hagberg K, Brånemark R, Gunterberg B, Rydevik B. Osseointegrated trans-femoral amputation prostheses: prospective results of general and condition-specific quality of life in 18 patients at 2-year follow-up. Prosthetics and Orthotics International 2008;32(1):29–41.
[16] Helgason B, Taddei F, Pálsson H, Schileo E, Cristofolini L, Viceconti M, et al. A modified method for assigning material properties to FE models of bones. Medical Engineering and Physics 2008;30(4):444–53.
[17] Helgason B, Perilli E, Schileo E, Taddei F, Viceconti M, Brynjólfsson S. Mathematical relationships between bone density and mechanical properties. Clinical Biomechanics 2008;23(2):125–46.
[19] Keaveny TM. Bone mechanics handbook. 2nd ed. Boca Raton, Florida: CRC Press; 2001 [chapter 16].
[20] Keyak JH, Fourkas MG, Meagher JM, Skinner HB. Validation of an automated method of three-dimensional finite element modeling of bone. Journal of Biomedical Engineering 1993;15(6):505–9.
[21] Klein CP, Patka P, van der Lubbe HB, Wolke JG, de Groot K. Plasma-sprayed coatings of tetracalciumphosphate, hydroxyl-apatite, and alpha-tcp on titanium alloy: an interface study. Journal of Biomedical Materials Research 1991;25(1):53–65.
[22] Lee W, Frossard L, Zhang M. Load mechanics in external and bone-anchored prostheses. In: Biomedical engineering conference. 2006. p. 71–4.
[23] Lee WCC, Frossard LA, Hagberg K, Haggstrom E, Brånemark R, Evans JH, et al. Kinetics of trans-femoral amputees with osseointegrated fixation performing common activities of daily living. Clinical Biomechanics 2007;22(6):665–73.
[24] Lee W, Frossard L, Pearcy M, Cairns N, Brånemark R. Evidence-based rehabilitation of amputees using osseointegrated prostheses: applications of finite element modeling. In: Proceedings of the 12th international conference on human–computer interaction. 2007.
[25] Lee W, Frossard L, Cairns N, Brånemark R, Evans J, Adam C, et al. Finite element modeling to aid in refining the rehabilitation of amputees using osseointegrated prostheses. In: Proceedings of the 12th international conference on human–computer interaction. 2007.
[26] Lengsfeld M, Schmitt J, Alter P, Kaminsky J, Leppek R. Comparison of geometry-based and voxel-based finite element modeling and experimental validation. Medical Engineering and Physics 1998;20(7):515–22.
[27] Les CM, Keyak JH, Stover SM, Taylor KT. Development and validation of a series of three-dimensional finite element models of the equine metacarpus. Journal of Biomechanics 1997;30(7):737–42.
[28] Morgan EF, Bayraktar HH, Keaveny TM. Trabecular bone modulus-density relationships depend on anatomic site. Journal of Biomechanics 2003;36(7):897–904.

[29] Ota T, Yamamoto I, Morita R. Fracture simulation of the femoral bone using the finite-element method: how fracture initiates and proceeds. Journal of Bone and Mineral Metabolism 1999;17(2):108–12.
[30] Robinson KP, Brånemark R, Ward D. Chapter 53: Future developments: osseointegration in transfemoral amputees. In: Smith DG, Michael JW, Bowker JH, editors. Atlas of amputations and limb deficiencies: surgical, prosthetic and rehabilitation principles. 3rd ed. American Academy of Orthopaedic Surgeons; 2005. p. 673–81.
[32] Schwefel HP. Evolution and optimum seeking. New York: Wiley; 1995.
[34] Søballe K, Hansen ES, Brockstedt-Rasmussen H, Bünger C. Hydroxyapatite coating converts fibrous tissue to bone around loaded implants. The Journal of Bone and Joint Surgery 1993;75(2):270–8.
[35] Sullivan J, Uden M, Sooriakumaran S. Rehabilitation of the trans-femoral amputee with an osseointegrated prosthesis: the united kingdom experience. Prosthetics and Orthotics International 2003;27(2):114–20.
[36] Taddei F, Schileo E, Helgason B, Cristofolini L, Viceconti M. The material mapping strategy influences the accuracy of CT-based finite element models of bones: an evaluation against experimental measurements. Medical Engineering and Physics 2006;29(9):973–9.
[37] Taddei F, Viceconti M, Manfrini M, Toni A. Mechanical strength of a femoral reconstruction in paediatric oncology: a finite element study. Proceedings of the institution of mechanical engineers, part H, vol. 217. Journal of Engineering in Medicine 2003:111–9.
[38] Viceconti M, Bellingeri L, Cristolfolini L, Toni A. A comparative study on different methods of automatic mesh generation of human femurs. Medical Engineering and Physics 1998;20(1):1–10.
[39] Viceconti M, Brusi G, Pancanti A, Cristofolini L. Primary stability of an anatomical cementless hip stem: a statistical analysis. Journal of Biomechanics 2005;39(7):1169–79.
[40] Viceconti M, Pancanti A, Dotti M, Traina F, Cristofolini L. Effect of the initial implant fitting on the predicted secondary stability of cementless stem. Medical and Biological Engineering and Computing 2004;42(2):222–9.
[41] Viceconti M, Ricci S, Pancanti A, Capello A. Numerical model to predict the long-term mechanical stability of cementless orthopaedic implants. Medical and Biological Engineering and Computing 2004;42(6):747–53.
[42] Ward D, Robinson KP. Chapter 24: Osseointegration for the skeletal fixation of limb prostheses in amputation at the trans-femoral level. In: Brånemark P-I, editor. The osseointegration book—from calvarium to calcaneus. Quintessenz Verlag-GmbH; 2005. p. 463–75.
[43] Xu W, Crocombe AD, Hughes SC. Finite element analysis of bone stress and strain around a distal osseointegrated implant for prosthetic limb attachment. In: Proceedings of the institution of mechanical engineers, part H, 214. 2000. p. 17–26.
[44] Xu W, Xu DH, Crocombe AD. Three-dimensional finite element stress and strain analysis of transfemoral osseointegration implant. In: Proceedings of the institution of mechanical engineers, part H, vol. 220. 2006. p. 661–70.
[45] Zhang M, Don X, Fa Y. Stress analysis of osseointegrated transfemoral prosthesis: a finite element model. In: Conf Proc IEEE Eng Med Biol Soc, vol. 4(1–4). 2005.
p. 4060–3.
[46] Lee W, Frossard L, Hagberg K, Häggström E, Lee Gow D, Gray S, et al. Magnitude and variability of loading on the osseointegrated implant of transfemoral amputees during walking. Medical Engineering and Physics 2008;30(7):825–33.

Fig. 1. (a) The simplified bone/implant system. Parameters were set to R =16mm, r = 8 mm, r4 =1mm, e =60mm, L0 =50mm, L1+ L3 = 230.5 mm, L2=20mm and L4 = 112 mm. r1, r2, r3 and L5 and were variables in the optimization process. (b) Simplified FE model. The load (P) was applied at the height of the femoral head and the model was fixed at the distal end of the abutment.

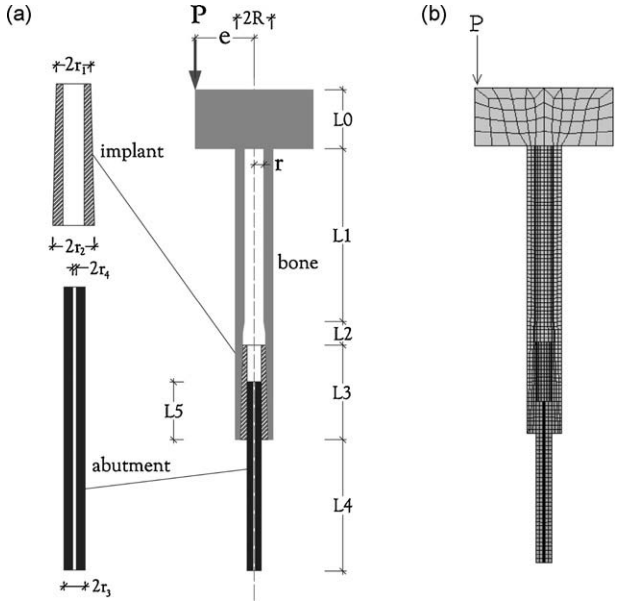

Fig. 2. Measured load cell forces (above) and moments (below) for subject 2. The x-, y-and z-axes are the medial–lateral, anterior–posterior and inferior–superior axes, respectively. HC: heel contact, TO: toe off, Max: maximum combined load.

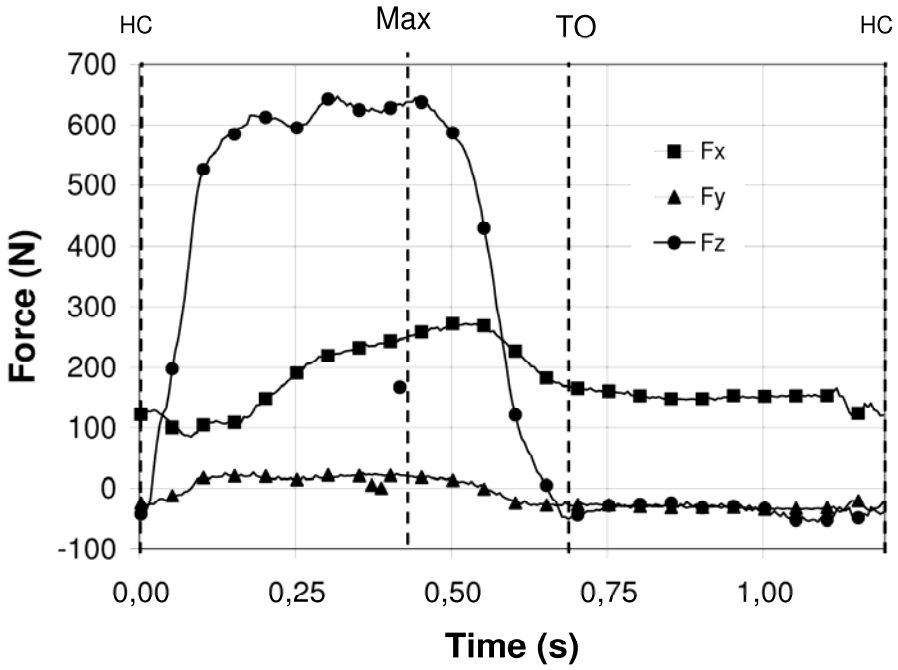

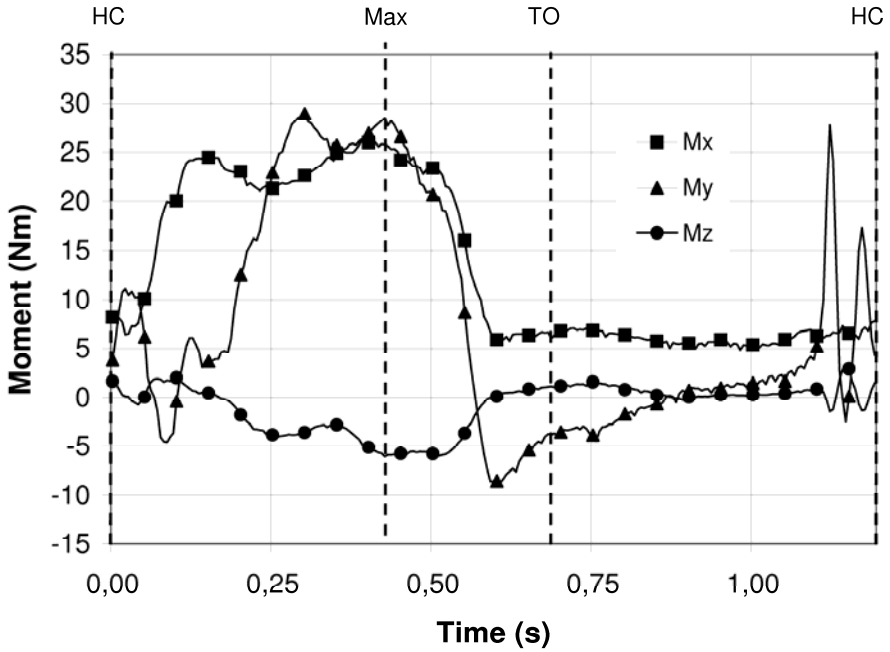

Fig. 3. (a) The 3D FE beam model that was used to calculate the loads that were applied to the subject-specific model (b). Average moment of inertia and Young's modulus for the femoral shaft was used for all elements in the beam model. The loads from the gait measurements were applied at the distal end of the beam model and reactions at three locations in the proximal end of the model calculated. The reactions were then applied at the exact same locations on the subject-specific model which was supported at the distal end of the abutment.

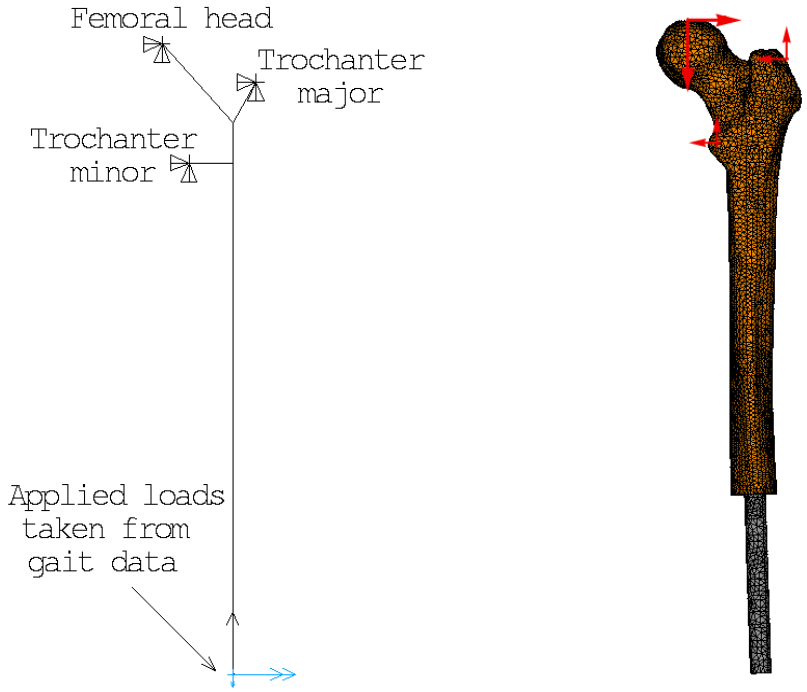

(a) (b)

Fig. 4. Average risk of failure for a complete gait cycle for the subject-specific model. RFb: risk of failure in bone according to Eq. (5), RFTi: risk of failure in implant/abutment according to Eq. (6). The dashed vertical line is drawn at the time of maximum average risk of failure (t = 0.42 s).

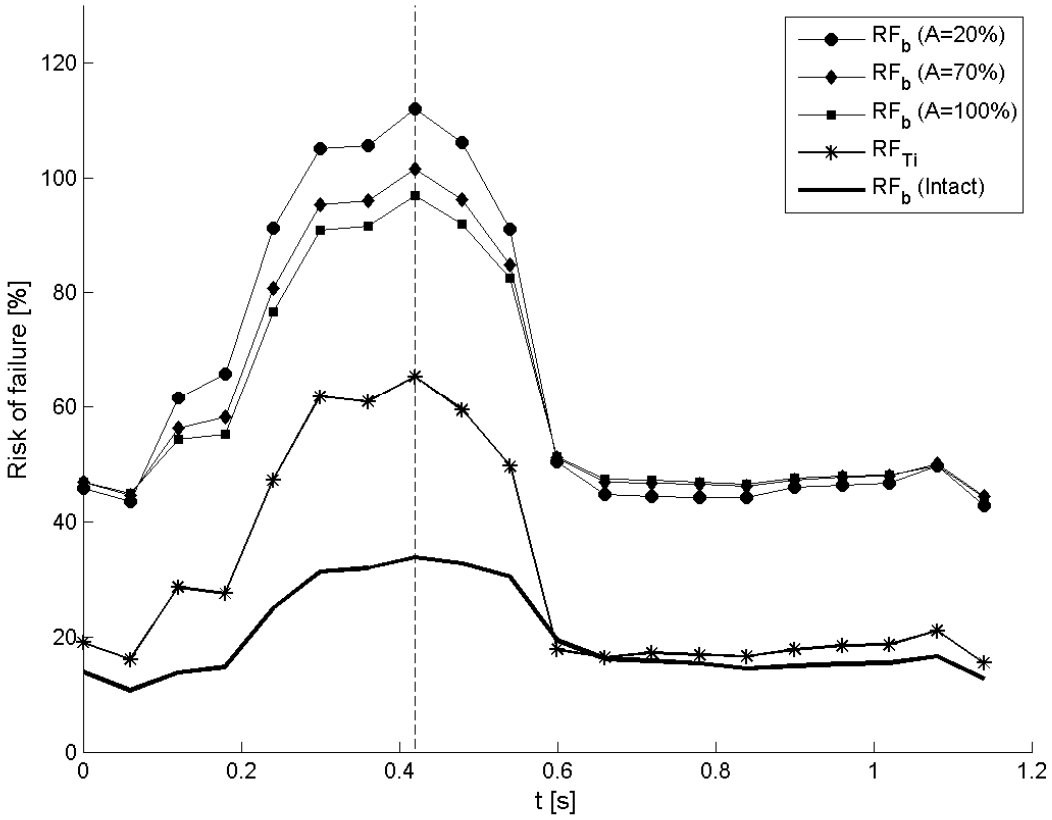

Fig. 5. Von Mises stress distribution, at maximum load in the region of interest for A = 100% bone implant contact. Units are in MPa.

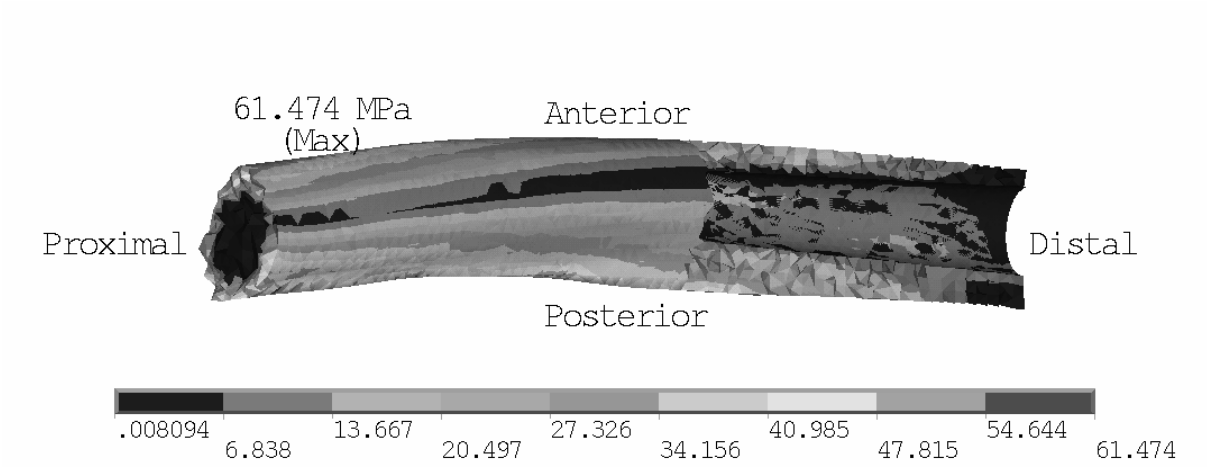

Table 1: Results from the optimization of the simplified FE model. L3, r1, r2, r3 and L5 are defined according to figure 1. Optimum search was carried out in two independent trials for each value of L3 with one hundred FE simulations in each trial. Pmax is the maximum load bearing capacity according to eq. (4) from both trials.

L_3 (mm)	r_1 (mm)	r_2 (mm)	r_3 (mm)	L_5 (mm)	P_{max} (N)
40	9.3	11.5	7.5	34.4	958
60	9.3	12.2	7.0	37.2	1002
80	9.3	11.3	6.5	55.4	1014
100	8.0	12.6	5.6	51.3	803
120	8.0	10.8	6.3	27.7	892

Table 2: Maximum average risk of failure during gait for bone (RF_b) and Titanium (RF_{tit}) for the subject specific FE model (at t=0.42s).

Case	RF_b (%)	RF_{tit} (%)
Intact femur	34	-
A=20%	112 ± 57	65 ± 0
A=70%	102 ± 19	65 ± 0
A=100%	97	65